MedLeak: Multimodal Medical Data Leakage in Secure Federated Learning with Crafted Models

Shanghao Shi
Virginia Tech
Arlington, VA, USA

Md Shahedul Haque
Virginia Tech
Arlington, VA, USA

Abhijeet Parida
Children's National Hospital
Washington, D.C., USA

Chaoyu Zhang
Virginia Tech
Arlington, VA, USA

Marius George Linguraru
Children's National Hospital,
George Washington University
Washington, D.C., USA

Y. Thomas Hou
Virginia Tech
Blacksburg, VA, USA

Syed Muhammad Anwar
Children's National Hospital,
George Washington University
Washington, D.C., USA

Wenjing Lou
Virginia Tech
Arlington, VA, USA

Abstract

Federated learning (FL) allows participants to collaboratively train machine learning models while keeping their data private, making it ideal for collaborations among healthcare institutions on sensitive datasets. However, in this paper, we demonstrate a novel privacy attack called MedLeak, which allows a malicious participant who initiates the FL task as the server to recover high-quality site-specific private medical images and text records from the model updates uploaded by clients. In MedLeak, a malicious server introduces an adversarially crafted model during the FL training process. Honest clients, unaware of the insidious changes in the published model, continue to send back their updates as per the standard FL training protocol. Leveraging a novel analytical method, MedLeak can efficiently recover private client data from the aggregated parameter updates. This recovery scheme is significantly more efficient than the state-of-the-art solutions, as it avoids the costly optimization process. Additionally, the scheme relies solely on the aggregated updates, thus rendering secure aggregation protocols ineffective, as they depend on the randomization of intermediate results for security while leaving the final aggregated results unaltered.

We implement MedLeak on medical image datasets MedMNIST, COVIDx CXR-4, and Kaggle Brain Tumor MRI datasets, as well as the medical text dataset MedAbstract. The results demonstrate that the proposed privacy attack is highly effective on both image and text datasets, achieving high recovery rates and strong quantitative scores. We also thoroughly evaluate MedLeak across different attack parameters, providing insights into key factors that influence attack performance and potential defenses. Furthermore, we perform downstream tasks, such as disease classification, using the recovered data, showing no significant performance degradation compared to the original training samples. Our findings validate the need for enhanced privacy measures in federated learning systems, particularly for safeguarding sensitive medical data against powerful model inversion attacks.

CCS Concepts

• **Security and privacy**; • **Computing methodologies** → **Machine learning**;

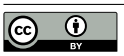
Keywords

Federated Learning, Model Inversion Attack, Medical AI Privacy.

ACM Reference Format:
Shanghao Shi, Md Shahedul Haque, Abhijeet Parida, Chaoyu Zhang, Marius George Linguraru, Y. Thomas Hou, Syed Muhammad Anwar, and Wenjing Lou. 2025. MedLeak: Multimodal Medical Data Leakage in Secure Federated Learning with Crafted Models. In *ACM/IEEE International Conference on Connected Health: Applications, Systems and Engineering Technologies (CHASE '25), June 24–26, 2025, New York, NY, USA.* ACM, New York, NY, USA, 12 pages. https://doi.org/10.1145/3721201.3721375

1 Introduction

Federated learning (FL) has developed as a key enabling technology for the future implementation of AI-powered medical diagnosis and treatment systems [1, 5, 8, 20, 21, 24, 28, 31]. FL allows medical centers to collaboratively train machine-learning models for various clinical tasks such as disease classification and clinical diagnosis, without sharing private patient information. This is crucial because medical centers are bound to preserve patient privacy and their data usage is strictly restricted in many clinical applications in accordance with regulatory guidelines. Under the FL framework, distributed training is set up in a way where hospitals that own private clinical data usually serve as clients, and a server – either hosted at one of the collaborating sites or maintained by a third party, integrates the model updates received from each client to orchestrate the federated learning paradigm. There are multiple open source (such as NVFLARE [29] and OpenFL [27]) as well as commercial platforms (such as Rhino FCP [33]), designed to



This work is licensed under a Creative Commons Attribution 4.0 International License.
CHASE '25, New York, NY, USA
© 2025 Copyright held by the owner/author(s).
ACM ISBN 979-8-4007-1539-6/2025/06
https://doi.org/10.1145/3721201.3721375

streamline the implementation of FL. During the FL training process, only the model updates, which refer to either the gradients or parameter updates, are exchanged between the participant and the server, while the private training samples are kept securely at the clinical site. Therefore, when first introduced, federated learning was considered to be privacy-preserving and the model updates are regarded as safe vectors that hide training samples' private information [18, 25, 36, 37, 41].

Existing Privacy Attacks. Recent privacy attacks challenged the privacy-preserving property associated with FL. It is demonstrated that a curious or malicious parameter server can extract information related to the training samples such as their labels, membership information, and even the whole training sample using the model updates [9–11, 17, 19, 35, 40, 42, 44]. Of particular interest, the model inversion attacks (MIAs) [9, 11, 23, 32, 40, 44] are a type of privacy attack aiming to recover the original training images. They take the individual model updates provided by the clients as inputs and reverse them back to the local training samples. This could be detrimental in medical applications, where such an attack can reconstruct patient-specific data. Existing MIAs usually formulate this reverse process as an optimization problem and have been shown to achieve good recovery performance in recovering high-fidelity training images from the model updates, when enough optimization iterations are performed. This completely exposes the information that the FL system has been designed to protect.

However, existing optimization-based MIAs are facing serious scalability and efficiency challenges. In practice, they need the server to consume extensive resources (usually hundreds of computation seconds with large memory) to recover only a few images, making them virtually impractical for real-world systems. Further, such MIAs can also be prevented by a specialized multi-party computation (MPC) mechanism named secure aggregation (SA) protocol [4, 6, 26], whose fundamental idea is to use various cryptography primitives (e.g., secret sharing) to mask individual model updates with random values but keep their summation identical to the pre-masked value. In this way, the FL system can proceed to the training process without exposing *individual model updates*, preventing the MIAs from reversing them back to local training samples.

Our Attack. In this paper, we propose a novel attack name MedLeak that addresses the limitation of the existing works. Our attack design makes it very practical, which could be detrimental to privacy in existing FL systems. MedLeak is an efficient attack, capable of recovering hundreds of training samples in a batch from the victim client within just a few seconds. MedLeak can also break the SA protocols as it can recover the training samples directly from the *summation value* of the model updates even though the individual ones are cryptographically masked. In addition, MedLeak can be accomplished within one FL training round, making it very practical and stealthy. To further evade detection, the attacker can launch the attack in the initial FL training rounds to avoid hurting the FL training performance. A greedy attacker can even launch the attack multiple times during continuous training rounds to harvest as many local training samples as possible.

Technically, MedLeak is a two-phase attack including the attack preparation phase and the sample recovery phase. In the first phase, the attacker adds an additional two-linear layer module in front of the original model architecture and initializes the module with customized parameters before sending it to the clients. For the target victim, the attacker initializes the parameters of the two-layer module to form a "linear leakage" module with the help of an auxiliary dataset that has the same data format and distribution as the training samples. This "linear leakage" module is a powerful mathematical tool that can perfectly reverse its gradients back to its inputs, which are identical to the training samples because we place this module as the first component of the model architecture. For other clients, their two-layer modules' parameters are crafted to form a "zero gradient" module, aiming to zero out their gradients and model updates. By doing so the aggregated model update is identical to the model update of the victim because all the others are set to zero, rendering the SA protocols useless.

As medical data is usually composed of both image and text records, we explore and extend MedLeak's capability to recover both data modalities. Particularly, the recovery of medical text records is largely ignored in the existing literature and we are proposing *the first* work in this direction to our knowledge. Compared to medical images, the recovery of medical text records is more challenging because they are discrete natural language words with different paragraph lengths in the input space, resulting in completely different FL model architectures and parameter calculation methodologies. To address this challenge, we slightly modify and customize our attack to insert the malicious module after the embedding layer rather than at the front of the whole model to first launch the recovery word embedding vectors, and then further reverse these word embedding vectors back to input tokens (words).

We evaluated MedLeak on MedMNIST [39], COVIDx CXR-4 [34], Kaggle Brain Tumor MRI [22] datasets for medical images, and on the MedAbstract dataset [30] for medical text records. For medical images, we evaluated our attack performance using the recovery rate, structural similarity (SSIM) score, peak signal-to-noise ratio (PSNR) score, and attack time. Our results show that MedLeak achieves excellent performance on these datasets to recover hundreds of images simultaneously with high recovery rates and quantitative scores, with only a few seconds of execution time. On visual inspection, the recovered images are virtually indistinguishable from the original images. We compared the performance of MedLeak with three existing MIAs. Our results demonstrate that MedLeak achieves better quantitative scores and is comparatively much more efficient. We further fed the recovered images to downstream disease diagnosis tasks. Our results show that the recovered images achieved a classification performance close to the original images, validating the effectiveness of our attack. For medical text records, we evaluated our attack performance using the recovery rate, word error rate (WER), and attack time. The results show that MedLeak can accurately recover tens of long clinical data paragraphs (e.g., descriptions of patients' health conditions) spanning up to hundreds of words simultaneously. This highlights MedLeak's strong capability to recover non-image modality records effectively and efficiently.

In summary, in this paper we present the following contributions:

(1) We propose MedLeak, a novel and powerful MIA that is capable of recovering high-quality local training samples in large batches using model updates from FL clients efficiently, even

Table 1: A comparison between the existing MIAs and MedLeak with respect to their attack assumptions, efficiency, scales, capabilities, and attack generalizability.

Attacks	Attack Model	Attack Efficiency	Scale	Break SA?	Recover Text?	Targeted?
[11, 16, 38, 40, 42, 44]	Honest-but-curious	Low (Optimization-based)	10^1	No	No (Image-only)	No
[23]	Malicious server	Low (Optimization-based)	10^1	Yes	No (Image-only)	Yes
[9, 43]	Extra attack module	High (Mostly closed-form)	10^2 to 10^3	Yes	No (Image-only)	No
MedLeak	Extra attack module	High (Closed-form)	10^2 to 10^3	Yes	Yes	Yes

when state-of-the-art cryptography-based defense mechanisms such as secure aggregation are employed.

(2) Our attack represents a fundamental and practical privacy vulnerability of the medical FL system as it compromises individual clients' privacy. MedLeak can target both medical image and text data, demonstrating its broad applicability in the medical domain.

(3) We provide rigorous mathematical analysis and proof for our attack. Our proposed attack design is closed-form, hence avoids incurring any computation-intensive optimization and significantly reduces the computational costs when compared to existing MIAs.

(4) We implement MedLeak on medical images and text datasets under different practical assumptions in the FL systems. The results show that our attack can nearly perfectly recover different types of local training samples of the target victim.

2 Background

2.1 Federated Learning

We consider for each training round t, there are n clients denoted by $C = \{c_1, c_2, \cdots, c_n\}$ to be selected by the parameter server S to collaboratively train a global model $G = f_\theta : \mathcal{X} \to \mathcal{Y}$, with each client c_i holds a local dataset D_i. In detail, the parameter server S first publishes the global model parameters θ^t to the clients. Then each client trains the received global model G_t for L_i^t local rounds over D_i to generate its model update δ_i^t. Note that when $L_i^t = 1$, the model update δ_i^t can be replaced by the gradient g_i^t. After that, the client c_i sends the model update δ_i^t back to the server S and the server employs model aggregation (such as using the federated average (FedAVG) algorithm [18]) to conduct the training process:

$$\theta^{t+1} = \sum_{i=1}^{n} \alpha_i \delta_i^t, \tag{1}$$

where α_i is the weight assigned to client c_i. The summation of all weights $\{\alpha_i\}_{i:c_i \in C}$ is 1 and can be adjusted according to the size of local datasets D_i^t to avoid training bias. The server may also employ alternative aggregation strategies (such as FedSGD algorithm [18]) for model aggregation. In the following text, we will omit the notation t, because our attack and analysis are all conducted in a single FL training round.

Federated learning has been widely used in the healthcare domain, enabling different healthcare providers to collaborate with each other towards accomplishing the training of machine learning models for both natural language processing and imaging tasks [14, 15, 25]. Such clinical FL systems usually leverage the patients' private information as the local training datasets. These can be the patients' radiology scans, textual reports, and tabular records describing the patients' visits and health conditions. This information is considered to be highly private and sensitive and is protected by strict governance laws such as HIPPA and GDPR. The medical FL system is deployed to protect such privacy by ensuring that the sensitive data never leaves the firewalls within the healthcare sites during the model training process. However, herein we will demonstrate with MedLeak that the privacy-preserving property of current FL systems is under challenge.

2.2 Model Inversion Attacks

The model inversion attacks (MIAs) take the individual model updates δ_i as the inputs and aim to reconstruct them back to the local datasets D_i held by the clients. This reversion problem has been formalized as an optimization problem, represented as $\arg\min_{\hat{D}_i}[d(\nabla\hat{D}_i - \nabla D_i)]$, where $\hat{D}_i$ refer to randomly initialized dummy samples and $d()$ refers to a distance function such as the second norm distance. To solve this optimization problem, [44] utilizes the L-BFGS optimizer to reconstruct the dummy samples iteratively step by step until reaching a good optimization point. It is further improved by an analytical method that aims to recover the ground-truth labels of dummy samples from the gradients [42], which significantly eases the optimization task and helps accomplish better attack performance. Later works have improved the optimization tools and focus on recovering larger batches of images on more practical machine learning models such as the ResNet [11, 16, 38, 40]. However, their recovery sizes are still restricted to the scale of tens, representing a scalability challenge. Moreover, all the aforementioned MIAs require costly iterative optimization methods in their design, which introduce a very large overhead to recover each batch of input images. Further, these existing methods also cannot bypass the current SA protocols.

2.3 Secure Aggregation

To enhance the privacy of the federated learning systems, Bonawitz et al. [4] proposed a new type of specialized MPC mechanism named the secure aggregation (SA) protocols to fulfill an abstract function of masking individual model updates δ_i to u_i with random bits, while keeping the summation of the masked values $\sum_{i=1}^n u_i$ identical to those of the pre-masked values $\sum_{i=1}^n \delta_i$. Therefore, despite variations of detailed cryptographic design, all SA protocols ensure that the server *cannot* obtain the individual model updates δ_i to launch any model inversion attacks, but can proceed with the FL training process with the aggregated model update $\sum_{i=1}^n u_i$, which is identical to $\sum_{i=1}^n \delta_i$. Since its initial introduction, the SA protocols have been continuously refined to incorporate other properties including communication efficiency, drop-out resilience [3, 7, 12, 13],

and security against malicious clients [6, 26], making it the current state-of-the-art privacy protection mechanism for FL systems.

Secure Aggregation under Challenge: Under the honest-but-curious attack model, the SA protocols have proven to be secure against various MIAs. However, recent works adopt a stronger attack model to assume a *proactive* attacker that modifies the global model's parameters and even its architecture before publishing it to the clients. Under this assumption, [23] proposed a novel attack that retrieves a target individual model update from the aggregated result, breaking the SA protocols. The fundamental idea is to craft the model parameters to adversarial models and distribute different adversarial models to different clients strategically. The adversarial models are crafted to ensure that only the model update of the victim client is preserved while all the others are zeroed out. The limitation of this attack is that it incorporates a costly optimization process in its design, which introduces too much attack overheads. [9] proposed another attack method to add crafted modules before the original model architecture. These additional modules are crafted with delicate mathematical designs to ensure that the model gradients can be perfectly reversed back to inputs whenever the server receives any model updates. The limitation of this attack is that the attacker cannot link the recovered images to their owners, which means the SA protocols still preserve a certain level of privacy, known as "privacy by shuffling". Later, [43] addressed this issue by designing a more complex adversarial module composed of convolutional and linear layers before the original model to identify the client associated with the recovered images. However, using a computer vision-related architecture prohibits the attack from being adopted to recover text records.

2.4 Attack Summary and Comparison

In Tab. 1, we summarize and compare the existing MIAs according to their attack assumptions, efficiency, scales, capabilities, and generability. In our design, we adopt the active attacker assumption to break the SA protocol and simultaneously address various limitations of the existing works. In particular, we aim to address the following three problems: 1) *attack efficiency*-our attack shall not employ any computation-intensive optimization process to incur large overheads; 2) *attack effectiveness*- our attack's capability of recovering high-quality local training samples from the *aggregated model updates* and attribute them back to individual clients even when SA protocols are incorporated, and 3) *attack generality*- our attack can be applied to traditional image recovery tasks as well as text recovery task (currently less explored).

3 Threat Model

In Fig.1 we demonstrate the threat model of our attack. We consider the parameter server S to be a malicious party that is curious about the training samples held by clients (e.g., private patient images or text records). We consider the parameter server to be a proactive attacker and can actively modify model parameters and architectures from G to $\hat{G}$ to achieve the attack goals, following the same assumption as [9, 23, 32, 43]. We assume the communication channels between the server and clients are secured and all messages can be authenticated. We assume the state-of-the-art SA protocols are in place and the server can only get access to

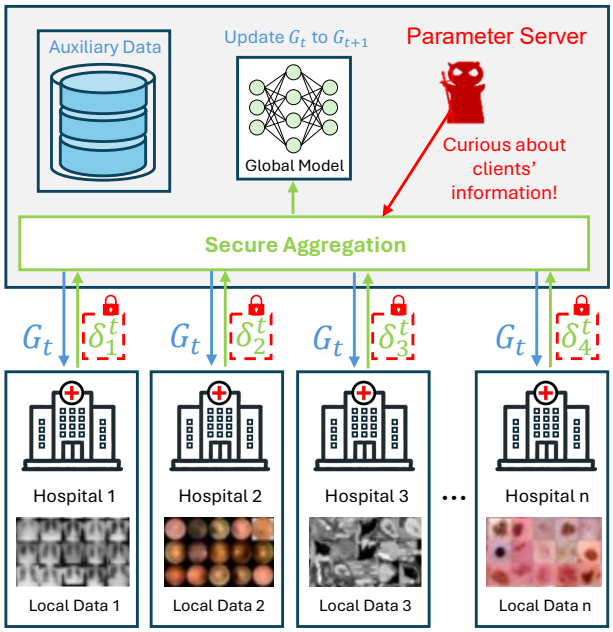


Figure 1: Threat Model. The server is considered to be a malicious attacker. The secure aggregation protocol is considered to be in place to protect the individual model updates.

the *aggregated model updates* $\sum_{i=1}^{n} \delta_i$ without knowing anything about the individual values δ_i. We consider the attacker is able to collect or obtain an auxiliary dataset D_{aux} that has the same data format and can represent the target dataset well. The attacker can leverage various online resources such as publicly available datasets, image searching tools, and image generative tools to fulfill this requirement. For our use case, the availability of public chest X-rays and medical text datasets makes this task trivial. The goal of the attacker is to recover the local data samples of a target client c_{target} just from the aggregated model updates $\sum_{i=1}^{n} \delta_i$. This can be mathematically expressed as: $D_{target} = Reverse(\sum_{i=1}^{n} \delta_i, \hat{G})$.

4 Attack Method

4.1 Attack Overview

As we assume the attacker only possesses the already-masked aggregated model updates $\sum_{i=1}^{n} \delta_i$ under the protection of the SA protocol, it is very challenging to identify an end-to-end method that directly reverses the aggregated results back to local training samples D_{target}. To address this, we decompose the complex recovery problem into two different distinct tasks including the *individual model update retrieval* and *efficient model update reversion* tasks. The first task aims to retrieve the individual model update of the victim from the aggregated model updates, thus breaking the SA protocol. The second task aims to reverse the individual model update back to local samples, achieving the recovery sub-problem.

To accomplish them, we require the attacker to place an additional two-linear-layer module L_{adv} with the rectified linear unit (ReLU) activation function in between at the beginning of the original global model, i.e. $\hat{G} = G \oplus L_{adv}$. The dimension of this module is

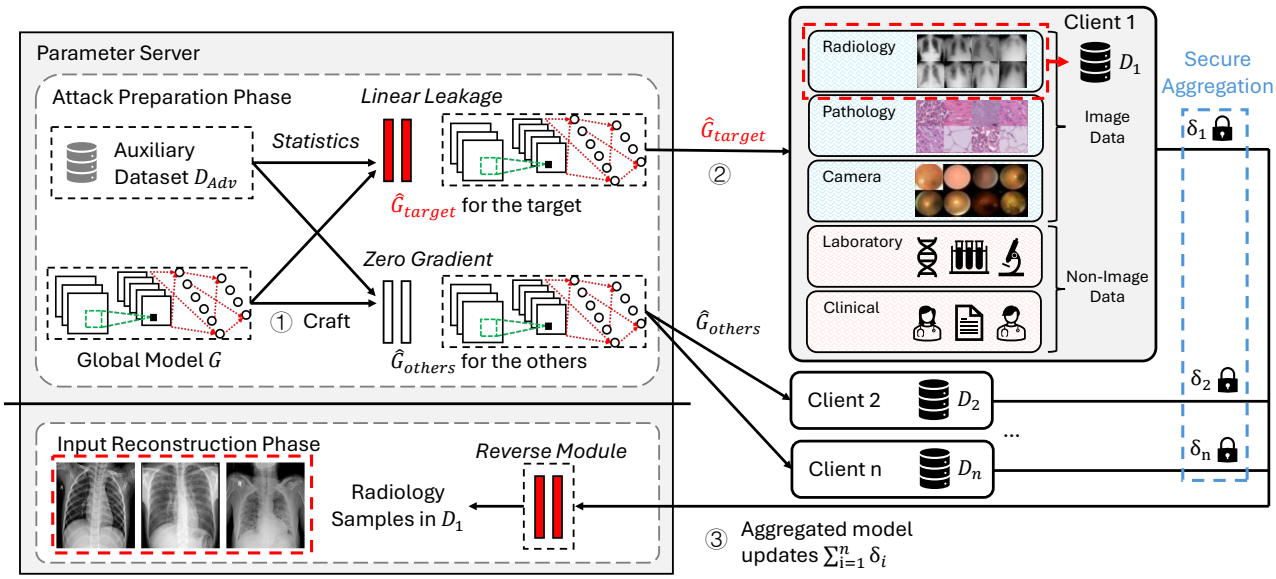


Figure 2: MedLeak attack flow. MedLeak is a two-phase attack. In the first preparation phase, the attacker generates the adversarial global model. In the second reconstruction phase, the attacker sends the adversarial models to the clients and recovers the local samples when it receives their feedback. MedLeak can reconstruct both image and non-image data and this figure demonstrates the reconstruction of the medical radiology images.

identical to the image dimension. We require the attacker to initialize the parameters of the linear module L_{adv} to form different adversarial modules and distribute them to different clients accordingly. For all the other clients except the victim, the attacker crafts the "zero gradient" modules L_{zero} to ensure that the gradients and model updates of these clients are always zero, i.e. $\hat{G}_{others} = G \oplus L_{zero}$. By doing this, the attacker guarantees that only the model update of the victim client is exposed, accomplishing task one. For the victim client, the attacker crafts a "linear leakage" module L_{linear}, aiming to reverse its model update back to local training samples efficiently, i.e. $\hat{G}_{target} = G \oplus L_{linear}$. This module requires an auxiliary dataset to help generate essential parameters and can ensure that samples are *perfectly recovered* with a mathematical proof, accomplishing task two. Detailed attack flow and module designs are introduced in the next section.

4.2 Detailed Attack Flow

We demonstrate the attack flow in Fig.2. MedLeak is a two-phase attack including 1) attack preparation and 2) sample reconstruction phases. In the attack preparation phase, the attacker crafts the adversarial global model $\hat{G}$ and initializes it with different model parameters including L_{zero} and L_{linear} (step ①) before publishing them to different clients (step ②). Then in the second phase, the attacker collects the aggregated model updates and uses an analytical method to reverse it back to local training samples (step ③). MedLeak can be used to reconstruct both medical image and non-image data. In the following parts, we will first introduce the overall attack flow and detailed design components via the image data reconstruction task, and then introduce how MedLeak can be customized to accomplish the text reconstruction task.

Attack Preparation: In this phase, the attacker crafts both the "linear leakage" module and "zero gradient" module once at the outset. Both modules require the estimation of essential parameters of a representative auxiliary dataset D_{aux}. In detail, the attacker first estimates the cumulative density function (CDF) of the brightness feature $h(x)$ of the auxiliary dataset D_{aux}, denoted by $\psi(h(x))$, to represent the CDF of the local training dataset (which is unavailable), where x refers to the input vector. After that, the attacker divides the distribution ψ into equally k bins by calculating $h_j = \psi^{-1}(j/k)$ where $j \in \{1, 2, \cdots, k\}$, ψ^{-1} refers to the inverse function of ψ, and k equals to the neuron number of the first linear layer. By doing so, the brightness of a random input vector x denoted by $h(x)$ will have the same probability of falling into each bin. This bin vector $\mathbf{H} = [h_1, h_2, \cdots, h_k]$ is the key vector to form both attack modules.

Linear Leakage Module: Assuming the weight and bias matrix of the two-layer module L_{adv} are w_1, b_1 and w_2, b_2 respectively. For the target victim, the attacker initializes the "linear leakage" module L_{linear} with the following steps: (1) having w_1's row vectors all identical to $\left[\frac{1}{d}, \frac{1}{d}, \cdots, \frac{1}{d}\right]$, where d refers to the dimension of the input images, resulting in calculating the brightness feature on each neuron when the local training images are sent into the model during the FL training process; (2) having the bias b_1 identical the opposite value of $\mathbf{H}$, i.e.,$b_1 = -\mathbf{H}$; (3) having all row vectors of w_2 the same.

Zero Gradient Module: The "zero gradient" module is initialized in the same way as the "linear leakage" module except in step (2), in which the attacker has the bias vector b_1 equal to $\mathbf{H}' = -[h_k, h_k, \cdots, h_k]$. By doing so, the output of the first linear layer will always be smaller than zero because h_k is the largest possible brightness and all possible input x's brightness is smaller

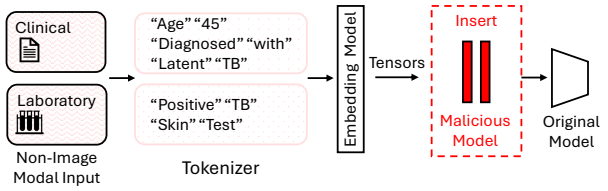


Figure 3: An example of how the medical text classification system works and where to insert the malicious modules.

than it. Considering we use the ReLU activation function after the first layer, the input to the second layer and the gradients of the first layer shall always be zero because of the ReLU function's mathematical property. This results in zero model updates for all clients except the target victim. Therefore, the aggregated model updates are identical to the model update of the victim client, i.e. $\sum_{i=1}^{n} \delta_i = \mathbf{0} + \mathbf{0} + \cdots + \mathbf{0} + \delta_{target} = \delta_{target}$, exposing the model update of the target victim.

Sample Reconstruction: The sample reconstruction phase can be treated as the actual *attack phase*, in which the parameter server disseminates the crafted global models $\hat{G}$ to all clients and recovers the local samples of the target victim D_{target} according to the aggregated model updates $\sum_{i=1}^{n} \delta_i$ provided by all clients.

More specifically, with the help of the "zero gradient" module, the aggregated model update $\sum_{i=1}^{n} \delta_i$ the attacker obtains is identical to the model update of the victim client δ_{target}, even though the SA protocols are in place. We further argue that the attacker can accurately estimate the gradients from the model update δ_{target} as it equals local iterations of the gradients [18, 32]. We define the gradients of the first two layers of the target victim as g_{w_1}, g_{b_1} and g_{w_2}, g_{b_2} respectively. The attacker can calculate the following equation to reconstruct the input samples, for $l \in \{1, 2, \cdots, k\}$:

$$(g_{w_1}^{(l+1)} - g_{w_1}^{(l)})/(g_{b_1}^{(l+1)} - g_{b_1}^{(l)}), \tag{2}$$

where specially we have $g_{w_1}^{(k+1)}$ and $g_{b_1}^{(k+1)}$ equal zero.

Analysis: Equ. 2 creates k recovery bins to recover input images. Fortunately, when $k \geq m$, where m refers to the size of the target dataset, each local training sample in the dataset will be *perfectly recovered* within a certain bin ranging from 1 to k. Here perfect recovery means that the inputs are analytically calculated through closed-form mathematical equations. A rigorous mathematical proof for this property is provided in the next section. However, when $k < m$, there will be recovery conflicts, and some recovered samples are mixed with each other in certain bins, resulting in degraded recovery rates and quality. We argue this does not mean the total failure of the image reconstruction task. We will later demonstrate that in this scenario the attack performance gradually decreases and the attack remains to achieve decent performance when attack parameter k is about the same scale as m.

We regard the attack parameter k as the key factor that affects reconstruction performance. Fortunately, from the attacker's perspective, this parameter is controlled and adjustable. The attacker can have a larger k (i.e. craft larger linear layers) for large datasets and a smaller one for small datasets according to different attack scenarios to ensure that there are enough recovery bins for all samples.

Regarding attack complexity, both the attack preparation and sample reconstruction phases only involve closed-form mathematical calculations that are super efficient to be conducted.

4.3 Proof of Correctness

Without the loss of generality, we use x_p to denote the local input sample. Considering the input x_p falls in the p^{th} largest bin, i.e. the brightness of x_p denoted by $h(x_p)$ satisfies $h_p < h(x_p) < h_{p+1}$. We have the following equation holds:

$$\begin{aligned}
\frac{g_{w_1}^{(p+1)} - g_{w_1}^{(p)}}{g_{b_1}^{(p+1)} - g_{b_1}^{(p)}} &= \frac{\nabla_{w_1(p+1)} L - \nabla_{w_1(p)} L}{\nabla_{b_1(p+1)} L - \nabla_{b_1(p)} L} \\
&= \frac{\frac{\partial L}{\partial y_{p+1}} \frac{\partial y_{(p+1)}}{\partial w_{1(p+1)}} - \frac{\partial L}{\partial y_p} \frac{\partial y_{(p)}}{\partial w_{1(p)}}}{\frac{\partial L}{\partial y_{p+1}} \frac{\partial y_{(p+1)}}{\partial b_{1(p+1)}} - \frac{\partial L}{\partial y_p} \frac{\partial y_{(p)}}{\partial b_{1(p)}}} \\
&= \frac{\sum_{v=1}^{p} \frac{\partial L}{\partial y_{p+1}} x_v - \sum_{v=1}^{p-1} \frac{\partial L}{\partial y_p} x_v}{\sum_{v=1}^{p} \frac{\partial L}{\partial y_{p+1}} - \sum_{v=1}^{p-1} \frac{\partial L}{\partial y_p}} \\
&= \frac{\frac{\partial L}{\partial y_p} x_p}{\frac{\partial L}{\partial y_p}} = x_p
\end{aligned} \tag{3}$$

where L is the loss function, y is the output of the first linear layer, and $\frac{\partial L}{\partial y_{p+1}} = \frac{\partial L}{\partial y_p}$ because we let the row vectors of the w_2 matrix identical.

This equation implies x_p is perfectly recovered from the gradients of the first linear layer. Because $\mathbf{H}$ covers the whole distribution range of the brightness feature, each input image will fall into one bin and thus can be recovered in this way as long as the image number is smaller than k.

4.4 Text Data Reconstruction

The medical text records are usually natural language words with discrete values within the input space. They have different mathematical properties from the medical images which are continuous pixel values in the input space. As a result, the medical natural language processing (NLP) models usually have different model architectures and workflows compared to their vision counterparts. In Fig. 3, we demonstrate the architecture of a text classification model. More specifically, for an input sentence x, the model first converts it to a sequence of tokens $(t_1, t_2, \cdots, t_l)$, where l refers to the maximum length of the sentence. Then the tokens are fed into the embedding model to be converted into the word embedding vectors, represented by $z = [e_1, e_2, \cdots, e_l]^T$, where all word embedding vectors e_i have the same pre-defined embedding dimension. After that, the word embedding vectors are fed into the classification model to produce the output o.

Within this model architecture, our original attack strategy of placing the attack module in the front is not effective because the words are all discrete values and cannot be recovered in the same way as the continuous pixel values. Instead, we insert our attack module L_{adv} including both the "linear leakage" module L_{linear} for the target victim and the "zero gradient" module L_{zero} for the



Figure 4: Recovered examples from the COVIDx CXR-4 dataset, Kaggle Brain Tumor MRI dataset, and MedAbstract dataset. The original images are on the left and the recovered ones are on the right. The text samples are truncated due to space limitations. Recovery failure samples are marked in red rectangles.

others between the embedding layer and the classification model. In this way, according to our previous analysis, the attacker can successfully recover the embedding vectors $z = [e_1, e_2, \cdots, e_l]^T$ with the help of these attack modules. The next question is can the attacker further reverse the embedding vectors i.e. e_i back to the tokens t_i? Fortunately, the answer is yes. This is because the word embedding layer maps the discrete tokens into continuous embedding vectors in the embedding space similar to a "lookup table"; therefore, the attacker can simply select the word within the whole word vocabulary that minimizes the distance between the actual embedding vector and the calculated one to be the original token. In practice, we use a single Softmax layer to achieve this reverse function.

Analysis: Similar to the image recovery task, the performance of the text recovery task is largely affected by the number of recovery bins k. We assume during the FL training process, m text data samples are organized in a batch with each one having a maximum length of l words. We clarify that the maximum sentence length l does not affect the recovery performance as long as it is not super large (e.g. 10^4), which we will later justify in the experiment

Table 2: The reconstruction performance of MedLeak over different datasets and reconstruction batch sizes. The rate (sample recovery rate) is on a scale of 1.00

Batch Size	Dataset	Pixel Size	Rate	PSNR	SSIM	Time (in sec)
100	ChestMNIST(pneumonia)	28x28	1.0	112.574	0.99	0.742
	COVIDx CXR-4	224x224	0.951	120.795	0.99	6.022
	Kaggle Brain Tumor MRI	224x224	0.962	107.783	0.99	6.308
200	ChestMNIST(pneumonia)	28x28	0.960	102.722	0.99	0.936
	COVIDx CXR-4	224x224	0.891	114.982	0.99	7.003
	Kaggle Brain Tumor MRI	224x224	0.870	98.6421	0.99	6.738
300	ChestMNIST(pneumonia)	28x28	0.957	97.405	0.99	0.95
	COVIDx CXR-4	224x224	0.880	105.123	0.99	8.121
	Kaggle Brain Tumor MRI	224x224	0.845	96.722	0.99	7.181
400	ChestMNIST(pneumonia)	28x28	0.955	93.713	0.99	1.020
	COVIDx CXR-4	224x224	0.864	97.301	0.99	8.762
	Kaggle Brain Tumor MRI	224x224	0.804	93.179	0.99	8.042
500	ChestMNIST(pneumonia)	28x28	0.964	87.019	0.99	1.016
	COVIDx CXR-4	224x224	0.810	95.864	0.99	9.763
	Kaggle Brain Tumor MRI	224x224	0.796	92.954	0.99	8.767

section. The recovery performance is still largely determined by the relationship between m and k. When $k \geq m$, each embedding vector is perfectly recovered within one bin, which further leads to excellent text recovery performance. But when $k < m$, there will be recovery collisions within certain bins, and the text recovery performance drops.

5 Evaluation

5.1 Experimental Settings

We implemented MedLeak on the PyTorch platform. We ran all the experiments on a server equipped with an Intel Core i7-12700K CPU 3.60GHzX12, one NVIDIA GeForce RTX 3080 Ti GPU, and Ubuntu 20.04.6 LTS.

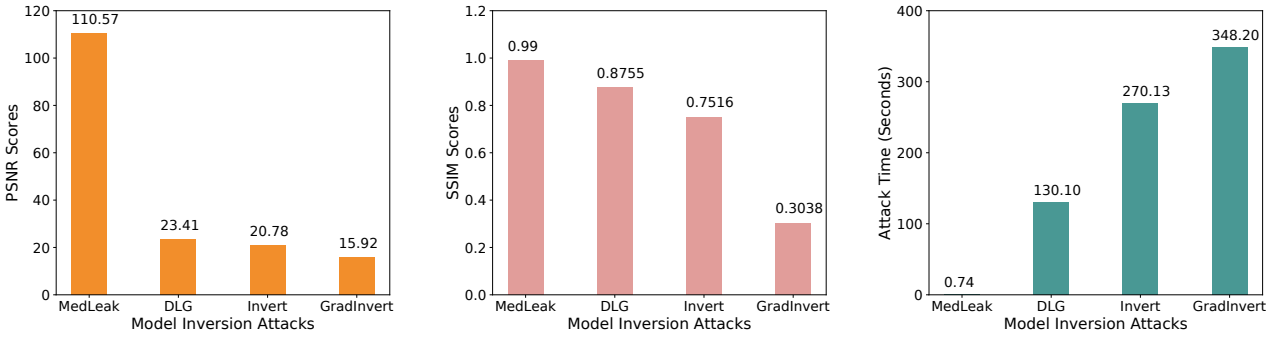
We considered the FL system to have 5 clients with one of them being the attack target per training round. We assumed each client would perform 5 local iterations before generating the individual model updates. We randomly selected 10% of the training set as the auxiliary dataset and aimed to recover samples in the test set, which have *no intersection* with the auxiliary dataset. We assumed the test set is partitioned and owned by the 5 clients locally to serve as the local datasets. For the defense mechanism, we considered the system to be protected by the SA protocol in [4]. Therefore, we cannot get access to the individual model updates (which have been cryptographically masked) and we launched our attack solely based on the aggregated model updates. Note that our attack can not only break the SA protocol in [4] because MedLeak breaks the abstract aggregation function of the SA protocols regardless of their implementation details. All SA mechanisms realizing the function can be broken, including [3, 6, 7, 12, 13, 26].

For the image recovery task, we chose the ChestMNIST dataset from the MedMNIST package [39], the COVIDx CXR-4 dataset [34], and the Kaggle Brian Tumor MRI dataset [22] as our experiment datasets. The ChestMNIST dataset comprises frontal view X-ray images (1×28×28) of 30805 unique patients with 14 disease labels and we selected data samples related to pneumonia to conduct our experiments, including 78468 training samples and 22433 testing samples. The COVIDx CXR-4 dataset also consists of frontal-view chest X-ray images with higher dimensions (resized to 1×224×224) and labels about whether the patient is COVID-positive. The training set contains 67863 images and the testing set contains 8482 images. The Kaggle Brain Tumor MRI Dataset contains 7023 images of human brain MRI images which are classified into 4 classes: glioma - meningioma - no tumor and pituitary. Its training set contains 5712 images and the testing set contains 1311 images.

We used four evaluation metrics including the recovery rate, the attack time, the peak signal-to-noise ratio (PSNR) score, and the structural similarity index measure (SSIM) score, following the convention of the existing works [9, 11, 40, 42, 44] to evaluate our attack over the image recovery task. More specifically, the successful recovery of samples was measured by observing the PSNR and SSIM scores between the original input samples and the reconstructed ones and checking whether those scores exceed a certain threshold th. In our work, we chose $th = 20$ for PSNR and $th = 0.9$ for SSIM because these thresholds are enough to ensure that the recovered images are visually clear for the attacker to extract all meaningful content from them.

For the text recovery task, we chose the MedAbstract dataset [30] as our experiment dataset. The MedAbstract data set consists of 14438 medical abstracts describing the patients' health conditions with each one consisting of a few hundred words. The patients' conditions are classified into 5 different classes including digestive system diseases, cardiovascular diseases, neoplasms, nervous system diseases, and general pathological conditions.

We used three evaluation metrics including the recovery rate, the word error rate (WER), and the attack time to evaluate MedLeak's performance over the text recovery task. Similar to the vision task, the recovery rate was defined as the ratio between the number of successfully recovered text samples achieving WERs lower than threshold 0.05 and the total sample number. Meanwhile, the WER was calculated as the portion of recovery failure words in text samples. In our experiment, we focused on the WER of the successfully recovered samples to evaluate their recovery quality.



(a) PSNR Scores. (b) SSIM Scores. (c) Attack Time (Seconds).

Figure 5: The attack performance comparison between MedLeak with other model inversion attacks.

Table 3: Downstream binary classification task on the COVID dataset with a pre-trained (with CXR-3 dataset) ViT model. TPR: True Positive Rate, TNR: True Negative Rate, ACC: Accuracy, AUC: Area Under Receiver Operating Characteristic curve, AUPR: Area Under Precision Recall curve.

Model	Image	AUPR	TNR	TPR	ACC	AUROC
ViT-S (SSL)	Original	0.937	0.800	0.857	0.829	0.905
	Recovered	0.921	0.900	0.710	0.805	0.919
ViT-S (Fine-tuned)	Original	0.974	0.970	0.930	0.950	0.969
	Recovered	0.965	0.886	0.938	0.912	0.966

5.2 Image Reconstruction Results

In Tab. 2, we demonstrate the performance of MedLeak over different recovery batch sizes (i.e. the number of samples recovered simultaneously held by the target victim) ranging from 100 to 500 images. We can observe that both the recovery rate (i.e. the ratio of successfully recovered images) and the quantitative scores (i.e. the PSNR and SSIM scores) decrease when the recovered batch size increases. This is expected because the larger the recovery batch size, the more difficult the recovery task to conduct. But in general, MedLeak achieves high recovery rates (> 0.8) and quantitative scores (PSNR> 80 and SSIM> 0.9) for all three datasets under all recovery batch sizes. Particularly, the SSIM scores (ranging from 0 to 1) remain to be 0.99 for all settings, because of the recovery excellency. This can be further verified by the recovered samples we visualized in Fig. 4, in which we plot the original images on the left and the recovered ones on the right. We find that the recovered images are of high quality and cannot be visually distinguished from the original ones, even for some detailed small marks and notations. In Tab. 2 we also demonstrate the attack time (in seconds). We find that the attack time is monotonically increasing with respect to the recovery batch size. For the largest batch size (i.e. 500 images) over the complex COVIDx CXR-4 dataset, it only takes the attacker less than 10 seconds to fulfill the recovery task, indicating that MedLeak is very effective.

5.3 Benchmark Comparison

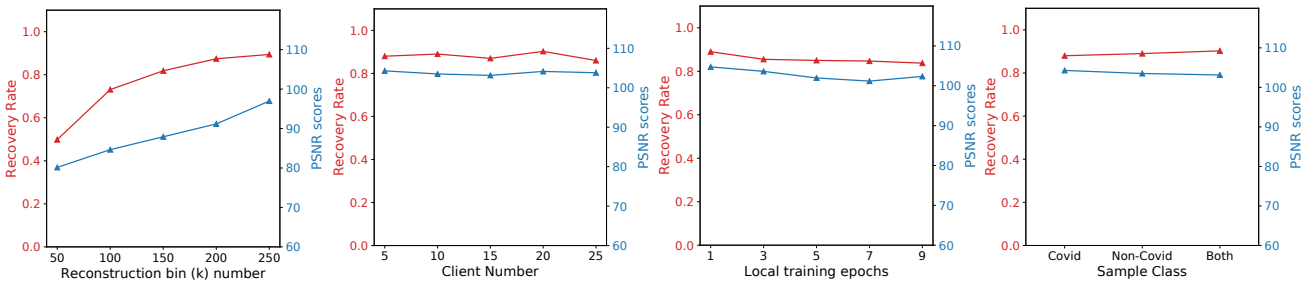
We compared MedLeak's attack performance with three optimization-based model inversion attacks (MIAs) including the DLG/iDLG [42, 44], InvertGradient [11], and GradInversion [40] attacks (denoted as DLG, Invert, and GradInvert respectively) over the MedMNIST dataset for one small batch of input images. We only focused on the image recovery task because all the existing attacks cannot be adapted to the text recovery task. We compared the PSNR scores, SSIM scores, and the attack time between the three attacks and our work. The results are demonstrated in Fig. 5. We can find that our attack achieves much better PSNR scores and SSIM scores than the existing MIAs, indicating that our attack can reconstruct samples with better quality. At the same time, our attack consumes significantly less time than the current MIAs. Particularly, the existing attacks consume a few hundred seconds to reconstruct one batch of samples, while our attack only requires less than one second, which reduces the current cost by two orders of magnitude. The reason why our attack is much more efficient is that our attack only involves closed-form mathematical calculations while the other three attacks require costly iterative-based optimization methods. However, there is no free lunch and we clarify that the three benchmark works adopt an honest-but-curious attack model, which does not allow the attacker to modify the model parameters and architecture as we did.

5.4 Vision Downstream Tasks

To further evaluate the performance of our attack on clinically relevant downstream tasks, we performed a binary disease classification (the detection of COVID-19) task on both the recovered samples and the actual samples. We used the state-of-the-art vision transformer model (ViT-S) (embedding size=368, number of heads=6, 22M parameters) pre-trained by self-supervised learning (SSL) technique on 30k COVIDx CXR-3 samples and fine-tuned on the RSNA-RICORD part of the dataset to perform the classification task [2] and evaluated it on the COVIDx CXR-4 dataset.

Table 4: The text reconstruction performance of MedLeak over a different number of text samples and experiment settings. The rate (sample recovery rate) is on a scale of 1.00. The "Embed Dim" refers to the embedding dimension.

Text Num	Max Length	Embed Dim	Rate	WER	Time (in sec)
20	200 words	64	0.9375	0.0004	0.2149
	300 words	64	0.9669	0.0009	0.3057
40	200 words	64	0.9212	0.0004	0.416
	300 words	64	0.9153	0.0018	0.6023
60	200 words	64	0.8729	0.0005	0.6341
	300 words	64	0.9083	0.002	0.9192
80	200 words	64	0.8228	0.0023	0.8331
	300 words	64	0.8540	0.0051	1.2308
100	200 words	64	0.755	0.0047	1.058
	300 words	64	0.7585	0.0052	1.514



(a) Recovery bins factor. (b) Client number factor. (c) Local training epochs factor. (d) Non-iid factor.

Figure 6: The recover performance of MedLeak over different practical attack factors.

We demonstrate the performance in Tab. 3. We use widely used machine learning metrics to evaluate the classification performance and we find that the recovered images achieve nearly the same performance as the original ones. This shows that our reconstruction process is highly successful in keeping all semantic meaning within the images and the reconstructed images can be used to perform any potential clinical analysis, which further indicates the severity of the privacy threat imposed by our attack. We consider it a very practical attack scenario for a curious party, which either can be the medical federated learning's participants or a third-party service provider (who provides the necessary platform, computation resource, and other FL infrastructures) to launch our attack to first reconstruct the sensitive medical images and then feed them to certain downstream analysis tasks to obtain further information about of the victims.

5.5 Text Reconstruction Results

In Tab. 4, we demonstrate MedLeak's performance on recovering medical text data under different batch sizes (ranging from 20 to 100) and data settings. More specifically, "text num" refers to the number of text samples recovered simultaneously in one batch, and "max length" refers to the maximum length of the text contents in the number of words. In our experiment, we fixed the length of each text sample for processing convenience. We truncated the samples when their lengths were longer than the maximum length and padded them when they were shorter. We also fixed the embedding dimension as the commonly used value 64. From the result, we can find that in general, MedLeak achieves decent text recovery performance under different settings to obtain high recovery rates (> 0.75), low WER scores (< 0.006), and short execution time within a few seconds. We observe that when the recovery batch size increases, the recovery rate decreases accordingly, meaning that recovering a larger batch of samples is more difficult. By comparing MedLeak's performance under different sample lengths (i.e. 200 v.s. 300 words), we further observe that a larger sample length triggers longer attack time, which approximately follows a linear relationship with the sample length. However, a larger sample length does not trigger any recovery performance drop. We still observe decent and stable recovery rates and WER scores when the sample length increases. In fact, the recovery rate even increases when the sample length is larger. This may be because longer samples maintain more semantic information and can be better separated and recovered.

5.6 Performance Affecting Factors

In this section, we investigate MedLeak's performance under different FL settings. We implemented the attack on the COVID CXR-4 dataset and evaluated the recovery rates and PSNR scores considering the following 4 factors: recovery bin number, client number, local training epoch, and non-iid data settings.

Recovery Bin Number: As we have discussed in Section 4. The recovery bin size k (i.e. neuron number of the first linear layer) can significantly affect the performance of MedLeak. In the experiment, we fixed the reconstruction batch size to 100 and changed the recovery bin k size from 50 to 250. We demonstrate the results in

Fig. 6(a). We find that both the recovery rates and PSNR scores are monotonically increasing with k and obtain relatively high quantitative scores when $k \geq m$. This is consistent with our theoretical analysis as more bins (larger k) will decrease the recovery conflict probability and increase the recovery success rates. In practice, the attacker can adjust the bin size according to local sample size to obtain decent attack performance.

Client Number: We increased the client number from 5 to 25 in our experiment. The results are shown in Fig. 6(b). We find that the attack performance is not affected by the FL client number. This indicates that our dis-aggregation attack phase is highly successful and the attacker can always obtain accurate model updates of the single victim client.

Local Training Epoch: We increased the local training epochs of the FL clients from 1 to 9. The results are demonstrated in Fig. 6(c). From the results we only observe very slight performance degradation when the FL clients conduct more local training epochs, demonstrating that our attack can be applied to both FedSGD and FedAVG settings.

Non-iid Data Distribution: We changed the class of samples held by the victim clients in our experiment including having COVID-only, non-COVID-only, and both type of samples. The results are shown in Fig. 6(d). We observe that the attack performance is not affected by the type of samples held by the victim client, indicating that MedLeak are applicable to both iid and non-iid settings.

6 Discussion and Future Work

Auxiliary Dataset: Using an auxiliary dataset is a commonly used prerequisite for state-of-the-art MIAs [9, 23, 32, 43]. Our attack takes the same assumption and its performance is also affected by the number and quality of samples in the auxiliary data D_{aux}. In the ideal case, the auxiliary dataset shall have the same data distribution as the target victim's local dataset, or the auxiliary dataset is more representative. It may be a challenge for the general vision tasks to find such a representative auxiliary dataset. However, for the medical data, this does not pose a critical barrier, since the radiology data (such as the CT scans) of humans are acquired in similar data format with common anatomical features. The attacker can obtain representative datasets released for research purposes in public domains. Moreover, because the attacker is a participant in the FL system, we consider they may even collude with others to obtain this auxiliary dataset.

Defense Mechanisms: An intuitive yet effective defense against our attack is for clients to proactively verify the consistency of model parameters and architectures during the FL training process, rather than blindly trust the privacy guarantees of FL systems and place full confidence in FL service providers—a trust that is prevalent in the current medical FL systems. However, we argue that our attack can be initiated during the initial training rounds, or even in the very first round, to maintain its stealthiness. This is because, in the early stages of training, when everything is randomly initialized, it becomes challenging for defenders to distinguish between malicious activities and benign patterns that arise from random initialization.

Another potential defense mechanism comes from the data synthesis perspective, leveraging the inherent bottleneck of MedLeak. Our comprehensive analysis reveals that the recovery bin size, denoted as k, plays a crucial role in affecting the attack performance. Specifically, when the sample size m is much larger than k, MedLeak's performance drops significantly. Based on this finding, the clients can generate large *mask sets* containing many images but not exposing anything related to the original private local samples to crowd the recovery bins. When the size of the mask set is large enough, there will be a lot of collisions within the bins, and the attacker can hardly recover anything. This defense strategy can also be employed for other attacks that face similar performance bottlenecks such as [9, 43]. However, the primary design challenge for such defense is to avoid causing any performance degradation when these mask sets are involved in the FL training process.

More than Linear Leakage: In this work, we leverage the fundamental "linear leakage" primitive as a powerful mathematical tool to help us accomplish our attack. However, we acknowledge that other types of model components such as the vision transformer [16], and convolutional layers [43] may also be exploited to reverse the model updates and leak private training data. These model components are integral to popular machine-learning models and can be exploited to launch the attack without the need to insert any additional malicious modules. This would make the attack more stealthy and adaptable for different victim models. However, designing such an analytical gradient reverse method is non-trivial, and we intend to explore such designs in future work.

7 Conclusion

In this paper, we present MedLeak–a novel MIA that targets current FL systems designed for healthcare applications using sensitive patient data. MedLeak can accurately and efficiently recover local training samples at a clinical site, resulting in unwanted leakage of private patient information. To achieve this, MedLeak requires the parameter server (i.e., the attacker) to actively craft additional adversarial attack modules before the global models. These adversarial models are designed with the mathematical guarantee to effectively break the secure aggregation protocol and efficiently recover hundreds of samples in a batch without relying on costly optimization methods when they are sent to the clients. We customize MedLeak to recover both image and textual data records, as clinical data usually comprises both types of samples, extending its applicability to wider healthcare-related FL systems. We implement MedLeak on multiple medical images and text datasets and our results highlight MedLeak's excellent attack performance under various real-world settings. Our attack exposes a practical vulnerability of the current medical FL systems, prompting the community to reconsider the privacy guarantees of these systems and to develop effective defenses against such advanced MIAs.

Acknowledgments

This work was supported in part by the Office of Naval Research under grants N00014-24-1-2730 and N00014-19-1-2621, the National Science Foundation under grants 2312447, 2247560, 2154929, 2332675, and 2235232, and Children's National Hospital, the Sanghani Center for AI and Data Analytics, and the Fralin Biomedical Research Institute at Virginia Tech.

References

[1] Mohammed Adnan, Shivam Kalra, Jesse C Cresswell, Graham W Taylor, and Hamid R Tizhoosh. 2022. Federated learning and differential privacy for medical image analysis. *Scientific reports* 12, 1 (2022), 1953.

[2] SM Anwar, A Parida, S Atito, M Awais, G Nino, J Kitler, and MG Linguraru. 2023. SPCXR: Self-supervised Pretraining using Chest X-rays Towards a Domain Specific Foundation Model. (2023).

[3] James Henry Bell, Kallista A Bonawitz, Adrià Gascón, Tancrède Lepoint, and Mariana Raykova. 2020. Secure single-server aggregation with (poly) logarithmic overhead. In *Proceedings of the 2020 ACM SIGSAC Conference on Computer and Communications Security*. 1253–1269.

[4] Keith Bonawitz, Vladimir Ivanov, Ben Kreuter, Antonio Marcedone, H Brendan McMahan, Sarvar Patel, Daniel Ramage, Aaron Segal, and Karn Seth. 2017. Practical secure aggregation for privacy-preserving machine learning. In *proceedings of the 2017 ACM SIGSAC Conference on Computer and Communications Security*. 1175–1191.

[5] Theodora S Brisimi, Ruidi Chen, Theofanie Mela, Alex Olshevsky, Ioannis Ch Paschalidis, and Wei Shi. 2018. Federated learning of predictive models from federated electronic health records. *International journal of medical informatics* 112 (2018), 59–67.

[6] Lukas Burkhalter, Hidde Lycklama, Alexander Viand, Nicolas Küchler, and Anwar Hithnawi. 2021. Rofl: Attestable robustness for secure federated learning. *arXiv e-prints* (2021), arXiv–2107.

[7] Beongjun Choi, Jy-yong Sohn, Dong-Jun Han, and Jaekyun Moon. 2020. Communication-computation efficient secure aggregation for federated learning. *arXiv preprint arXiv:2012.05433* (2020).

[8] Ittai Dayan, Holger R Roth, Aoxiao Zhong, Ahmed Harouni, Amilcare Gentili, Anas Z Abidin, Andrew Liu, Anthony Beardsworth Costa, Bradford J Wood, Chien-Sung Tsai, et al. 2021. Federated learning for predicting clinical outcomes in patients with COVID-19. *Nature medicine* 27, 10 (2021), 1735–1743.

[9] Liam Fowl, Jonas Geiping, Wojtek Czaja, Micah Goldblum, and Tom Goldstein. 2021. Robbing the fed: Directly obtaining private data in federated learning with modified models. *International Conference on Learning Representations (ICLR)* (2021).

[10] Chong Fu, Xuhong Zhang, Shouling Ji, Jinyin Chen, Jingzheng Wu, Shanqing Guo, Jun Zhou, Alex X Liu, and Ting Wang. 2022. Label inference attacks against vertical federated learning. In *31st USENIX security symposium (USENIX Security 22)*. 1397–1414.

[11] Jonas Geiping, Hartmut Bauermeister, Hannah Dröge, and Michael Moeller. 2020. Inverting gradients-how easy is it to break privacy in federated learning? *Advances in Neural Information Processing Systems* 33 (2020), 16937–16947.

[12] Xiaojie Guo, Zheli Liu, Jin Li, Jiqiang Gao, Boyu Hou, Changyu Dong, and Thar Baker. 2020. V eri fl: Communication-efficient and fast verifiable aggregation for federated learning. *IEEE Transactions on Information Forensics and Security* 16 (2020), 1736–1751.

[13] Swanand Kadhe, Nived Rajaraman, O Ozan Koyluoglu, and Kannan Ramchandran. 2020. Fastsecagg: Scalable secure aggregation for privacy-preserving federated learning. *arXiv preprint arXiv:2009.11248* (2020).

[14] Bill Yuchen Lin, Chaoyang He, Zihang Zeng, Hulin Wang, Yufen Huang, Christophe Dupuy, Rahul Gupta, Mahdi Soltanolkotabi, Xiang Ren, and Salman Avestimehr. 2021. Fednlp: Benchmarking federated learning methods for natural language processing tasks. *arXiv preprint arXiv:2104.08815* (2021).

[15] Ming Liu, Stella Ho, Mengqi Wang, Longxiang Gao, Yuan Jin, and He Zhang. 2021. Federated learning meets natural language processing: A survey. *arXiv preprint arXiv:2107.12603* (2021).

[16] Jiahao Lu, Xi Sheryl Zhang, Tianli Zhao, Xiangyu He, and Jian Cheng. 2022. APRIL: Finding the Achilles' Heel on Privacy for Vision Transformers. In *Proceedings of the IEEE/CVF Conference on Computer Vision and Pattern Recognition*. 10051–10060.

[17] Xinjian Luo, Yuncheng Wu, Xiaokui Xiao, and Beng Chin Ooi. 2021. Feature inference attack on model predictions in vertical federated learning. In *2021 IEEE 37th International Conference on Data Engineering (ICDE)*. IEEE, 181–192.

[18] Brendan McMahan, Eider Moore, Daniel Ramage, Seth Hampson, and Blaise Aguera y Arcas. 2017. Communication-efficient learning of deep networks from decentralized data. In *Artificial intelligence and statistics*. PMLR, 1273–1282.

[19] Milad Nasr, Reza Shokri, and Amir Houmansadr. 2019. Comprehensive privacy analysis of deep learning: Passive and active white-box inference attacks against centralized and federated learning. In *2019 IEEE symposium on security and privacy (SP)*. IEEE, 739–753.

[20] Dianwen Ng, Xiang Lan, Melissa Min-Szu Yao, Wing P Chan, and Mengling Feng. 2021. Federated learning: a collaborative effort to achieve better medical imaging models for individual sites that have small labelled datasets. *Quantitative Imaging in Medicine and Surgery* 11, 2 (2021), 852.

[21] Dinh C Nguyen, Quoc-Viet Pham, Pubudu N Pathirana, Ming Ding, Aruna Seneviratne, Zihuai Lin, Octavia Dobre, and Won-Joo Hwang. 2022. Federated learning for smart healthcare: A survey. *ACM Computing Surveys (Csur)* 55, 3 (2022), 1–37.

[22] Masoud Nickparvar. 2022. Brain Tumor MRI Dataset: A dataset for classifying brain tumors. https://www.kaggle.com/datasets/masoudnickparvar/brain-tumor-mri-dataset

[23] Dario Pasquini, Danilo Francati, and Giuseppe Ateniese. 2022. Eluding secure aggregation in federated learning via model inconsistency. In *Proceedings of the 2022 ACM SIGSAC Conference on Computer and Communications Security*. 2429–2443.

[24] Sarthak Pati, Ujjwal Baid, Maximilian Zenk, Brandon Edwards, Micah Sheller, G Anthony Reina, Patrick Foley, Alexey Gruzdev, Jason Martin, Shadi Albarqouni, et al. 2021. The federated tumor segmentation (fets) challenge. *arXiv preprint arXiv:2105.05874* (2021).

[25] Bjarne Pfitzner, Nico Steckhan, and Bert Arnrich. 2021. Federated learning in a medical context: a systematic literature review. *ACM Transactions on Internet Technology (TOIT)* 21, 2 (2021), 1–31.

[26] Krishna Pillutla, Sham M Kakade, and Zaid Harchaoui. 2022. Robust aggregation for federated learning. *IEEE Transactions on Signal Processing* 70 (2022), 1142–1154.

[27] G Anthony Reina, Alexey Gruzdev, Patrick Foley, Olga Perepelkina, Mansi Sharma, Igor Davidyuk, Ilya Trushkin, Maksim Radionov, Aleksandr Mokrov, Dmitry Agapov, et al. 2021. OpenFL: An open-source framework for Federated Learning. *arXiv preprint arXiv:2105.06413* (2021).

[28] Nicola Rieke, Jonny Hancox, Wenqi Li, Fausto Milletari, Holger R Roth, Shadi Albarqouni, Spyridon Bakas, Mathieu N Galtier, Bennett A Landman, Klaus Maier-Hein, et al. 2020. The future of digital health with federated learning. *NPJ digital medicine* 3, 1 (2020), 119.

[29] Holger R Roth, Yan Cheng, Yuhong Wen, Isaac Yang, Ziyue Xu, Yuan-Ting Hsieh, Kristopher Kersten, Ahmed Harouni, Can Zhao, Kevin Lu, et al. 2022. Nvidia flare: Federated learning from simulation to real-world. *arXiv preprint arXiv:2210.13291* (2022).

[30] Tim Schopf, Daniel Braun, and Florian Matthes. 2023. Evaluating Unsupervised Text Classification: Zero-Shot and Similarity-Based Approaches. In *Proceedings of the 2022 6th International Conference on Natural Language Processing and Information Retrieval* (Bangkok, Thailand) *(NLPIR '22)*. Association for Computing Machinery, New York, NY, USA, 6–15. https://doi.org/10.1145/3582768.3582795

[31] Micah J Sheller, Brandon Edwards, G Anthony Reina, Jason Martin, Sarthak Pati, Aikaterini Kotrotsou, Mikhail Milchenko, Weilin Xu, Daniel Marcus, Rivka R Colen, et al. 2020. Federated learning in medicine: facilitating multi-institutional collaborations without sharing patient data. *Scientific reports* 10, 1 (2020), 12598.

[32] Shanghao Shi, Ning Wang, Yang Xiao, Chaoyu Zhang, Yi Shi, Y Thomas Hou, and Wenjing Lou. 2025. Scale-MIA: A Scalable Model Inversion Attack against Secure Federated Learning via Latent Space Reconstruction. *Network and Distributed System Security (NDSS) Symposium* (2025).

[33] Keri Stephens. 2021. Rhino Health Raises 5 Million to Improve AI Workflows in Healthcare Using Federated Learning. *AXIS Imaging News* (2021).

[34] Linda Wang, Zhong Qiu Lin, and Alexander Wong. 2020. Covid-net: A tailored deep convolutional neural network design for detection of covid-19 cases from chest x-ray images. *Scientific reports* 10, 1 (2020), 19549.

[35] Lixu Wang, Shichao Xu, Xiao Wang, and Qi Zhu. 2019. Eavesdrop the composition proportion of training labels in federated learning. *arXiv preprint arXiv:1910.06044* (2019).

[36] Ning Wang, Yang Xiao, Yimin Chen, Ning Zhang, Wenjing Lou, and Y Thomas Hou. 2022. Squeezing more utility via adaptive clipping on differentially private gradients in federated meta-learning. In *Proceedings of the 38th Annual Computer Security Applications Conference*. 647–657.

[37] Kang Wei, Jun Li, Ming Ding, Chuan Ma, Hang Su, Bo Zhang, and H Vincent Poor. 2021. User-level privacy-preserving federated learning: Analysis and performance optimization. *IEEE Transactions on Mobile Computing* 21, 9 (2021), 3388–3401.

[38] Yuxin Wen, Jonas Geiping, Liam Fowl, Micah Goldblum, and Tom Goldstein. 2022. Fishing for user data in large-batch federated learning via gradient magnification. *arXiv preprint arXiv:2202.00580* (2022).

[39] Jiancheng Yang, Rui Shi, Donglai Wei, Zequan Liu, Lin Zhao, Bilian Ke, Hanspeter Pfister, and Bingbing Ni. 2023. MedMNIST v2-A large-scale lightweight benchmark for 2D and 3D biomedical image classification. *Scientific Data* 10, 1 (2023), 41.

[40] Hongxu Yin, Arun Mallya, Arash Vahdat, Jose M Alvarez, Jan Kautz, and Pavlo Molchanov. 2021. See through gradients: Image batch recovery via gradinversion. In *Proceedings of the IEEE/CVF Conference on Computer Vision and Pattern Recognition*. 16337–16346.

[41] Chen Zhang, Yu Xie, Hang Bai, Bin Yu, Weihong Li, and Yuan Gao. 2021. A survey on federated learning. *Knowledge-Based Systems* 216 (2021), 106775.

[42] Bo Zhao, Konda Reddy Mopuri, and Hakan Bilen. 2020. idlg: Improved deep leakage from gradients. *arXiv preprint arXiv:2001.02610* (2020).

[43] Joshua Christian Zhao, Atul Sharma, Ahmed Roushdy Elkordy, Yahya H Ezzeldin, Salman Avestimehr, and Saurabh Bagchi. 2023. LOKI: Large-scale Data Reconstruction Attack against Federated Learning through Model Manipulation. In *2024 IEEE Symposium on Security and Privacy (SP)*. IEEE Computer Society, 30–30.

[44] Ligeng Zhu, Zhijian Liu, and Song Han. 2019. Deep leakage from gradients. *Advances in neural information processing systems* 32 (2019).